

Thiocarboxylate functionalization of silver nanoparticles: effect of chain length on the electrical conductivity of nanoparticles and their polymer composites

Behnam Meschi Amoli,^{ac} Sarang Gumfekar,^{ac} Anming Hu,^b Y. Norman Zhou^{bc} and Boxin Zhao^{*ac}

Received 23rd May 2012, Accepted 6th August 2012

DOI: 10.1039/c2jm33280a

Thiocarboxylate-functionalized silver nanoparticles (NPs) were synthesized and characterized in terms of their thermal and electrical properties. Thiocarboxylic acids with chain lengths of 3 and 11 carbons were used to functionalize silver NPs, leading to the formation of NPs smaller than 5 nm. We found that silver NPs, functionalized with a short-chain acid, were twice smaller than those with a long-chain acid. Electrical conductivity measurements showed that the short-chain functionalized NPs were electrically conductive while the long-chain functionalized ones were nonconductive. The short-chain functionalized NPs were incorporated into a conventional electrical conductive adhesive (ECA) composite, consisting of micron-sized silver particles and an epoxy matrix to form a hybrid-designed ECA. The electrical conductivity measurements and SEM images of the cross-section of the cured hybrid composite showed that lower contents of the NPs (<20 wt% of the silver microparticles) increased the electrical conductivity due to the filling of NPs into the interstices of the micron-sized particles as well as their low sintering temperature, whereas higher NPs contents reduced the electrical conductivity because they clustered and increased the gaps between the microparticles. We attributed the positive effect of synthesized NPs on the electrical conductivity of the nanocomposite to their small size (<5 nm) and the specific design of the covering layer over the surface of NPs. These research findings provide insights into the relationship between the overall properties of the nanocomposites and the nanoparticles' surface chemistry, size and weight fractions.

Introduction

The unique electrical,^{1–4} thermal,⁵ optical^{6,7} and antibacterial^{8,9} properties of silver nanoparticles (NPs) have attracted extensive research interest with respect to their applications in the development of functional materials such as flexible electronic display,^{10,11} organic light-emitting devices¹² and biosensors¹³ at ever smaller scales. One critical step of many applications of NPs is to mix them into a polymer matrix to form nanocomposites; the NPs provide functionalities whereas the polymer matrix provides mechanical strength. A proper monolayer of surfactants is often needed to effectively cover the surface of NPs so as to reduce the surface energy, which in turn reduces the formation of aggregates and at the same time allows for loading more NPs in the polymeric matrix.¹⁴ Other than improving the dispersion of NPs in the polymeric matrix, the surface layer coated on NPs

negatively influences the desired functions of the NPs. For instance, the surfactant layers insulate NPs and reduce their intrinsic thermal and electrical conductivities; this situation limits the broader use of polymer nanocomposites as functional materials. This study focuses on the functionalization of silver NPs and their influence on the electrical conductivity of the silver NPs and their polymer composites.

Silver-filled polymer composites have been utilized as electrical conductive adhesives (ECAs) for device assembly. Compared to soldering and wire bonding technologies, electrical conductive adhesive bonding offers numerous advantages such as environmental friendliness (elimination of lead and flux cleaning), mild processing conditions, fewer processing steps, and especially, the fine pitch capability to make microjoining possible due to the availability of small size conductive fillers.^{15–19} However, the electrical conductivity of ECAs has always been a critical concern in this field because it is less than that of eutectic tin–lead solders. In the recent decades, there has been increasing interest in the application of silver NPs to enhance the electrical conductivities of conventional conductive adhesives filled with silver micro flakes.^{2,4,14,16,20–23} However, it has been reported that simply adding NPs has a negative effect on the overall conductivity because of the increased number of

^aDepartment of Chemical Engineering, University of Waterloo, 200 University Avenue West, Waterloo, ON, Canada N2L 3G1. E-mail: zhaob@uwaterloo.ca

^bDepartment of Mechanical and Mechatronics Engineering, University of Waterloo, 200 University Avenue West, Waterloo, ON, Canada N2L 3G1

^cWaterloo Institute for Nanotechnology, University of Waterloo, 200 University Avenue West, Waterloo, ON, Canada N2L 3G1

contact points.²⁴ A positive effect of NPs on the electrical conductivity of the polymer composite requires the sintering of NPs at high temperatures to reduce the number of contact points.^{14,21,25} Remarkable efforts are in progress to reduce the sintering temperature due to the thermal sensitivity of components in organic electronic devices.^{4,16,26,27} To date, the major focus has been on the application of silver NPs bigger than 20 nm. One possible reason is that the surface organic layer of NPs should be readily removed from the surface during the curing process in order to sinter NPs at lower temperatures.^{14,15,23} This condition usually needs the synthesis of NPs involving the physical adsorption of the organic layer on the surface of NPs, which leads to the formation of large NPs. Jeong *et al.*²⁰ investigated the incorporation of commercial 5 nm silver particles into the epoxy formulation and reported that adding a small amount of NPs (~2 wt%) improved the conductivity without the need of sintering, which highlights the positive effect of small NPs on the electrical conductivity of ECAs. This progress was promising; however, studies of silver NPs smaller than 10 nm in the development of conductive polymer composites are scarce in the literature. It may be because of the need for chemically stabilizing NPs during their synthesis to produce small NPs; the stabilizing agent could insulate the NPs, depending on its chain length and adsorption mechanism.

Varied chemicals including mono- or di-carboxylic acids,²⁸ sodium citrate,²⁹ amines³⁰ and alkanethiols^{31,32} have been used to produce functionalized NPs; the functional groups prevent them from forming aggregates. Since Brust *et al.*³³ developed a two-phase liquid–liquid system to synthesize alkanethiol-stabilized gold NPs, the synthesis and characterization of thiol-capped metal NPs have been subjected to a considerable research interest.^{34–37} Chen and Kimura developed a large scale synthesis method for the production of carboxylate-modified gold and silver NPs, which could be homogeneously dispersed in water and organic solvents while they could also be re-isolated as pure powder without any aggregation.^{38,39} Similar methods have been used considerably to synthesize metal NPs using thiocarboxylic acids.^{40–42} One of the striking features of stabilizing the metal NPs by thiocarboxylic acids is the production of very small (*i.e.*, less than 5 nm) and mono-dispersed NPs. The characteristic properties of this type of NPs such as size, size distribution, thermal and electrical properties can be controlled by the chemistry and coverage of the functional groups on the NPs surface. Although much research work has been performed to synthesize and functionalize silver NPs using different organic layers, to our knowledge there is no systematic study concerning the effect of this surface layer on the electrical properties of silver NPs and their corresponding polymer composites.

In this article, we investigated the effect of very small silver NPs as well as the specific roles of their surface layer on the electrical conductivity of a nano/micro hybrid composite adhesive. To do so, the conventional ECA consisting of 60 wt% Ag micron flakes in epoxy was used as a base composite because using only NPs leads to a non-conductive composite or requires a large amount of the NPs to be conductive, which is costly and not practical. Thiocarboxylic acids with different chain lengths were implemented to stabilize silver NPs. Although the chemically stabilized NPs have low conductivity, which limits their

application for the development of conductive nanocomposites or ECAs, we postulated that by reducing the number density and chain length of the stabilizing agent, the covering layer resistivity can be lowered and the NPs can be potentially used as reinforcing agents in ECAs. Furthermore, we hypothesized that the chemically stabilized NPs can be readily dispersed into epoxy and can be fused into a conductive network at a low temperature because of their small size. Our research findings revealed, for the first time that chemically stabilized NPs can improve the electrical conductivity of conventional ECAs at a relatively low curing temperature of 150 °C without the extra step of sintering at an elevated temperature.

Experiments and methods

Synthesis and chemical modification of silver NPs

11-Mercaptoundecanoic acid (MUA, ≥95 wt% Aldrich) and 3-mercaptopropionic acid (MPA, ≥99 wt% Aldrich) were used to stabilize silver NPs. These two thiocarboxylic acids differ in their chain lengths. The number of carbons in the backbone of MUA and MPA are 11 and 3 carbons, respectively. MPA-stabilized silver NPs (Ag–MPA) were synthesized following the established procedure.^{38,39,41} 40 mL of MPA (8 mmol) solution in tetrahydrofuran (THF) and 240 mL silver nitrate (340 mg, 2 mmol) (AgNO₃, ≥99 wt%, Aldrich) solution in THF–water (volume ratio: 5/1) were mixed dropwise. After 5 min, the initial transparent solution became blurry whitish along with the formation of small white clusters, which might be associated with the formation of an Ag–S bond.^{35,41} Subsequently, 20 mL of aqueous solution of sodium borohydride (20 mmol) (NaBH₄, ≥99 wt%, Aldrich) was added to the mixture, leading to an abrupt precipitation of dark-gray solid. In order to remove the unreacted materials, the precipitated sludge was washed three times by repeatedly dispersing in water and precipitating in THF followed by centrifugation at 8000 rpm for 30 min to remove the supernatant. The resultant gray solid was dispersed in 20 mL deionized (DI) water. MUA-stabilized silver NPs (Ag–MUA) were synthesized by the same procedure as Ag–MPA. 900 mg (4 mmol) of MUA was dissolved in 40 mL THF and added dropwise to the solution of AgNO₃, leading to the formation of a yellowish solution. The same sodium borohydride solution was used to reduce Ag⁺ ions, leading to the formation of a dark-brown solid. The same washing steps were applied for the synthesis of Ag–MPA. The final NPs were dispersed in 20 mL of DI water. All the glassware were cleaned prior to use; they were soaked in a 1 M solution of sodium hydroxide for 24 h, neutralized with acetic acid, and then rinsed with DI water. The DI water (resistivity > 10 MΩ cm at 25 °C; total organic carbon < 20 ppb) was obtained using a RiOs-DI Clinical system (Millipore Corporation).

Nanocomposite preparation

Diglycidyl ether of bisphenol A resin (DER™ 322) and triethylenetetramine (TETA) supplied by DOW chemical company (USA) were used as the epoxy base and hardener, respectively. The weight ratio of hardener to epoxy was 0.13. Two types of samples were prepared. One type contained only silver flakes (Aldrich, 10 μm); the other contained a mixture of the

synthesized NPs and silver flakes at different weight fractions. A small amount of isopropyl alcohol (6 wt% of the epoxy) was added to dilute the epoxy base before adding silver fillers. The total weight fraction of the silver varied from 60 to 70 wt% as listed in Table 1. The paste was mixed for 30 min using a vortex mixer followed by 1 h mixing in an ultrasonic bath. TETA hardener was then added and mixed using the vortex mixer for 10 min. The resultant paste was filled into a mold of $7 \times 7 \times 0.7$ mm³ ($L \times W \times D$) made using pieces of adhesive tape on a pre-cleaned microscope glass slide. To make a smooth surface and control the sample thickness, a clean copper plate was placed on top of the mold and the extra paste squeezed out. The samples were pre-cured for 30 min at 70 °C and then cured at 150 °C for 2 h. After curing, the copper plate and adhesive tape were manually peeled off.

Characterizations

Fourier transform infrared spectroscopy (FTIR) was performed using a Varian 640-IR machine to verify the chemical structure of the surface layer of silver NPs. A high resolution transmission electron microscope (HRTEM, JEOL 2010F FEG) was used to characterize the size and size distribution of the chemically stabilized silver NPs. To prepare TEM samples, one droplet of dilute dispersion of silver NPs in water (1 mg mL⁻¹) was dropped on a lacey/holey carbon copper grid and dried for 1 h in air. The TEM was operated at 200 kV and equipped with Gatan ultra scan imaging filter. Ultraviolet-visible spectroscopy (UV-vis) (UV-2501 pc, Shimadzu) was performed to confirm the formation and size distribution of synthesised NPs. The weight loss and surface coverage of NPs with thiocarboxylic acids were studied using thermogravimetric analysis (TGA) (TA instrument, Q500-1254). Samples of about 4 mg were placed in the TGA sample pan. Dynamic scan was performed from 40 to 600 °C with a heating rate of 20 °C min⁻¹ under nitrogen atmosphere. The morphologies of NPs and cured nanocomposites were examined by SEM (LEO 1530, Carl Zeiss NTS) operating at 5 and 15 kV. The bulk resistivity of the samples was measured using a four-point probe setup consisting of a probe fixture (Cascade microtech Inc.) and a source meter (Keithley 2440 5A Source Meter, Keithley Instruments Inc.)—see Fig. 1. The sheet resistance of the samples (R_s) was characterized by the drop in voltage when applying a constant current (10 mA). The electrical resistivity (ρ) of the nanocomposites was calculated using the following equation:

$$\rho = R_s t = \left(\frac{\pi t}{\ln 2} \right) \frac{V}{I} \Omega \text{ cm} \quad (1)$$

where t is the thickness of samples; I and V are the applied current and the measured voltage, respectively.

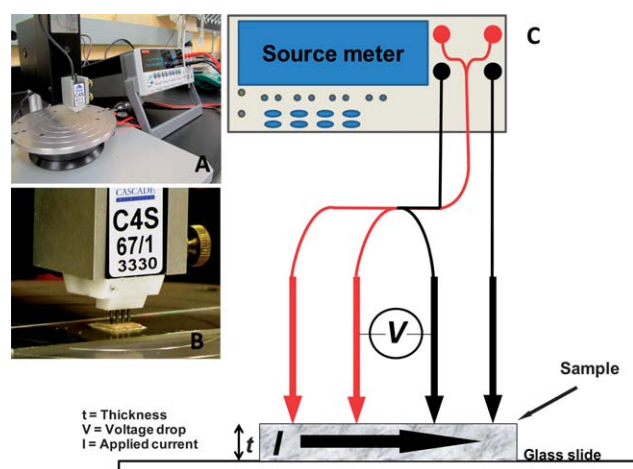


Fig. 1 (A) Electrical conductivity measurement setup consisting of a four-point probe and source meter, (B) a close-up image of the four-point probe, (C) schematic illustration of measuring the bulk resistivity of nanocomposites.

Results and discussion

Synthesis and characterization of silver NPs

The chemically stabilized Ag NPs were synthesized by the direct reduction of AgNO₃ using sodium borohydride in the presence of thiocarboxylic acid. Fig. 2A and B illustrate the synthesis mechanism. In step 1, the thiocarboxylic acid was added into the solution of the silver salt in THF–water; the acid partially reduced silver ions by forming coordinate bonds in which a pair of electrons of thiocarboxylic acid (R–S⁻, Lewis base) were donated to the Ag⁺ (Lewis acid), leading to the formation of a zero oxidation state of silver atoms (Ag⁰) that were chemically bonded to the hydrocarbon chains of the acid *via* Ag–S bond.³⁸ In step 2, a strong reducing agent, NaBH₄, was added to the suspension, which completely reduced the remaining silver ions to silver atoms (Ag⁰), resulting in the formation of silver NPs. The silver–acid compound, formed in step 1, self-assembled on the surface of growing silver NPs and limited the growth of the NPs nuclei. The carboxylate functional groups provided a steric repulsion to prevent NPs from aggregating and at the same time enabled them to get dispersed in water and/or other polar solvents. Fig. 2C shows typical TEM images of the MPA and MUA stabilized Ag NPs. Both NPs were roughly spherical and well dispersed. We measured the size of 100 randomly picked silver NPs; the size distributions of those NPs were shown in the inserted histograms of Fig. 2C. The Ag–MPA NPs' diameter ranged from 1 to 4 nm, while the majority was in the range of 1.5

Table 1 Weight fractions of silver NPs and flakes in nano–microparticles filled epoxy

Sample	Ag flakes (wt%)	Ag NPs (wt%)	$K = \frac{\text{Ag NPs}}{\text{Ag flakes}}$	Total weight fraction of fillers
1	60	0	0	60
2	53	11	0.2	64
3	48	19	0.4	67
4	44	26	0.6	70

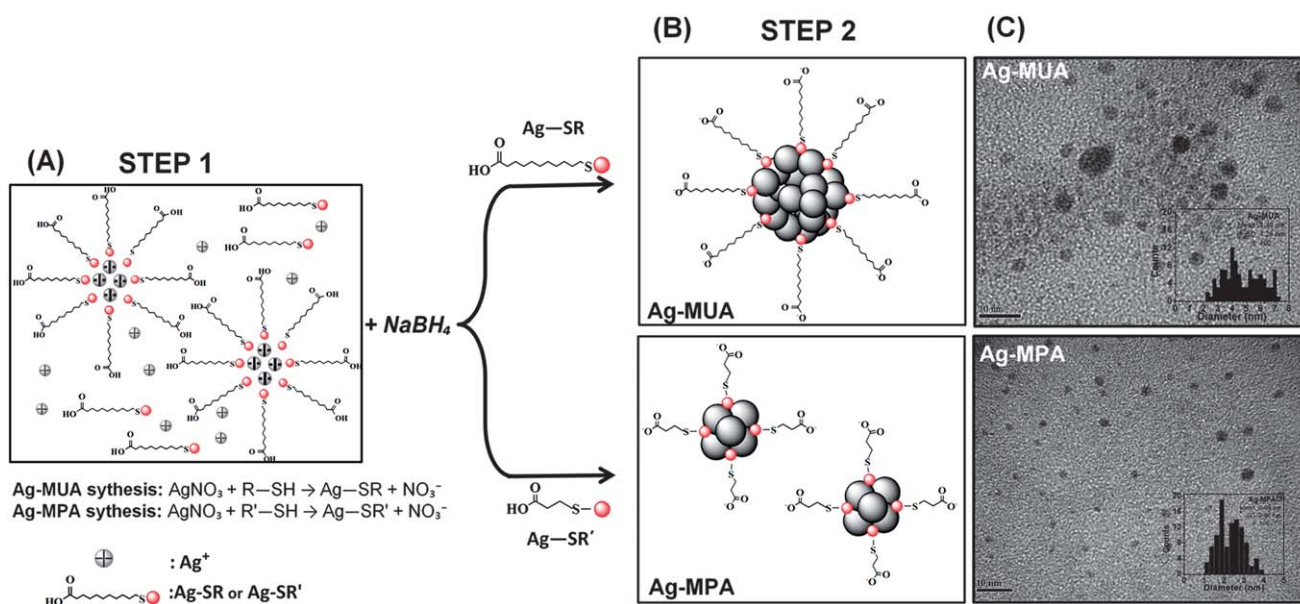


Fig. 2 Synthesis of silver nanoparticles: (A) step 1 – self assembly of thiocarboxylic acid on the surface of growing Ag NPs and partial reduction of Ag^+ ions by thiocarboxylic acid, (B) step 2 – formation of NPs reduced by a strong reducing agent (the NPs were capped by self-assembled thiocarboxylate groups), and (C) typical TEM images and histograms of synthesized NPs.

to 3 nm, giving an average diameter of 2.09 ± 0.66 nm. The diameter of the long-chain-stabilized NPs (Ag-MUA) ranged from 2 to 8 nm, giving an average diameter of 4.49 ± 1.28 nm. It is interesting to notice that NPs capped with the short chain acid (MPA) are smaller with a much narrower size distribution than the NPs capped with a long chain acid (MUA). Although the tuning of NPs size with the variation of the ratio of acid to NPs precursor (AgNO_3) has been known in the literature,^{39,41} to the best of our knowledge there is no particular study of the effect of chain lengths on the size of thiocarboxylate stabilized silver NPs. These results showed that the different chain lengths of the functional groups gave NPs of different sizes. We attribute the effect of chain lengths to the nature of the synthesis method. Although the exact mechanism is not clear, we considered the following two possible reasons. The first one might be related to the strength of acids. The proton (attached to the sulphur) of MPA is much closer than that of MUA to the electronegative carboxylic group (located at the end of the chain); this situation makes MPA a stronger acid than MUA. Thus, MPA can reduce a larger amount of silver ions in step 1; consequently less amount of silver ions remain in the system to grow the NP core. The second reason is related to the possible self-assembly mechanism of thiocarboxylic acids. The longer chain of MUA can form a larger micelle-like structure than the short chain of MPA, providing a larger space for NPs to grow their nuclei.

UV-Visible spectroscopic analyses were further performed to investigate the nature of the chemically stabilized NPs. Fig. 3 shows the optical spectra of both Ag-MPA and Ag-MUA NPs in aqueous solutions. Normally, metal NPs bigger than 2 nm have a strong and broad optical excitation peak in the UV-visible spectrum corresponding to the surface plasmon bonds (SPB).⁴³ The symmetrical feature of the SPB for both Ag-MPA and Ag-MUA suggested a uniform and homogenous dispersion of NPs in water since silver NPs aggregates cannot show any peak.⁴⁴ As

shown in Fig. 3, the SPB peaks were observed at wavelengths of 412 and 436 nm for Ag-MPA and Ag-MUA, respectively. Note that the SPB peak of pure silver NPs occurs between 380 and 390 nm.⁴⁵ These huge red shifts in the position of SPB peaks are because of the presence of a grafted organic layer on the surface of NPs.⁴⁶ The red shift in the position of the maximum absorption of Ag-MUA compared to that of Ag-MPA was also expected. Malinsky *et al.*³⁶ studied the effect of chain lengths on the optical properties of alkanethiol capped Ag NPs and reported the SPB peak would red shift 3 nm for every carbon atom in the alkane chain backbone. It is also known that the features of SPB of metal NPs depend on the size and size distribution in which the SPB of larger NPs moves to higher wavelengths compared to that of smaller ones.⁴⁷ Hence, the observed red shift for Ag-MUA was attributed to the longer chain of MUA.^{30,46}

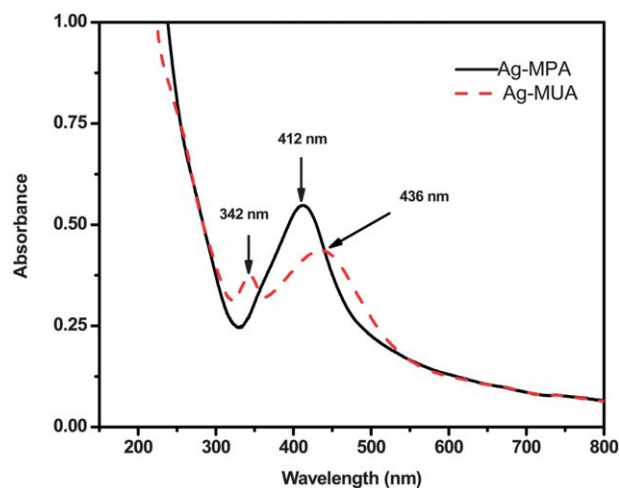


Fig. 3 UV-visible spectra of Ag-MPA and Ag-MUA NPs.

Beside the peak at 436 nm, Ag–MUA has another peak at 342 nm. Dell' Erba *et al.*⁴¹ reported a similar peak at 342 nm. They attributed this small peak to the presence of some silver clusters in the system. However, this small peak was not observed in the spectrum of Ag–MPA, perhaps because the size distribution of Ag–MPA was narrower than that of Ag–MUA as estimated from the TEM results. Furthermore, we checked the stability of NPs by comparing the UV-visible spectra of one-month aged samples with that of the fresh sample. As shown in Fig. 4, the features of the spectra for both samples did not change after one month, suggesting the surface carboxylate groups formed strong hydrogen bonding with water molecules, which made NPs quite stable in aqueous medium.³⁹

The chemical adsorption or grafting of thiocarboxylic acids on the surface of NPs was examined by FTIR. With the exception of liquid MPA, the analyses were performed in the solid state of all the other samples. Fig. 5 shows the spectra of pure acids and the functionalized NPs.⁴⁸ The broad peak at 3000 cm^{-1} for liquid MPA corresponds to some free water absorbed from the atmosphere. In the spectra of pure MUA and MPA, there are two small peaks centered at 2543 and 2558 cm^{-1} , belonging to the S–H stretching bond, which disappeared in the spectra of grafted NPs. It confirms that the thiol groups of the acids were attached to the surface of silver NPs *via* the formation of sulphur–silver bonds. The distinct peaks at 1691 and 1712 cm^{-1} for pure MUA and MPA (in the range of 1680–1720 cm^{-1}) belong to the carbonyl group of carboxylic acids. The peaks at 1559 and 1418 cm^{-1} for Ag–MUA, and at 1554 and 1403 cm^{-1} for Ag–MPA (Fig. 5) are, respectively, assigned to asymmetric and symmetric vibrations of carboxylate groups, confirming the existence of carboxylate groups on the surface of silver NPs which has been expected to be in the structure of the covering layer. The strong and sharp peaks at 2916 and 2845 cm^{-1} in the spectra of both pure MUA and Ag–MUA correspond to the asymmetric and symmetric stretching of methylene groups, respectively.

We take an analogy to the FTIR analysis of typical hydrocarbons such as polyethylene (PE) to obtain insights about the crystallinity of the surface layers on the synthesized NPs.⁴⁹ For dissolved PE in a solvent whose hydrocarbon chains are randomly oriented, the asymmetric and symmetric stretches of methylene have broad peaks at 2928 and 2856 cm^{-1} whereas for solid PE with a highly packed and crystalline structure these peaks became sharper and were at lower wavenumbers (*i.e.*, 2920

and 2850 cm^{-1}).⁴⁹ Applying an analogous information to the spectra of Ag–MUA, and considering the same methylene peak for Ag–MUA as the methylene peak of solid PE, it can be inferred that the long chain, attached to the surface of Ag–MUA NPs, might be in a crystalline form. These two peaks are not significant for the short-chain acid stabilized NPs. The crystalline structure of Ag–MUA was also reflected in the appearance of the NPs dry powder; Ag–MUA NPs dry powders were shiny and rigid while Ag–MPA NPs were fluffy and soft, as can be seen in Fig. 6.

TGA was performed to investigate the thermal properties and the amount of stabilizing agents on the surfaces of Ag–MPA and Ag–MUA. Fig. 7 shows the weight-loss vs. temperature plots for the pure MUA, Ag–MPA and Ag–MUA. Note that the pure MPA is a liquid at room temperature, so its analysis with TGA was not practical. The TGA of pure MUA showed thermal decompositions occurring between 130 and 300 °C, during which there was a 92% weight-loss; the other 8% weight loss occurred between 300 and 350 °C. There were two main weight-loss transition points for both Ag–MUA and Ag–MPA. Due to the presence of some pure MUA and moisture in the system, there was a small weight-loss before 300 °C for Ag–MUA. The first main transition of Ag–MUA occurred between 300 and 360 °C, having about 4 wt% weight-loss, which might be attributed to the amount of MUA physisorbed on the surface of silver NPs. The second main transition of Ag–MUA, having a larger weight-loss (~24 wt%), was observed at 437 °C and continued up to 490 °C. This large amount of weight-loss is attributed to decomposition of chemisorbed organic materials.⁵⁰ As for the Ag–MPA, its thermal decomposition started at 130 °C; the weight decreased by only 3 wt% until 270 °C because of the decomposition of some non-bonded MPA or absorbed water in the system. As the temperature increased, similar to Ag–MUA, Ag–MPA displayed two main thermal decomposition steps. The decomposition of physically adsorbed MPA occurred between 270 and 350 °C, having an approximately 7 wt% of the total weight-loss. The decomposition of chemically adsorbed MPA occurred between 400 and 470 °C, having 11 wt% weight-loss, which was almost half that of Ag–MUA. Further comparison of the TGA curves of Ag–MUA and Ag–MPA shows that the thermal decompositions of Ag–MPA started and finished at lower temperatures. It appears that the chemical functionalization of silver NPs using the long-chain acid was more effective than the short-chain acid,

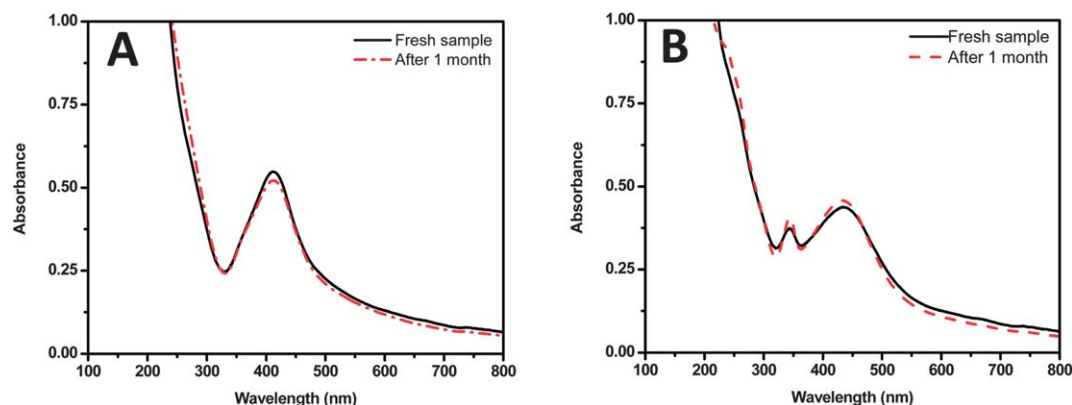


Fig. 4 UV-visible spectra of fresh and one-month aged NPs aqueous dispersions: (A) Ag–MPA NPs and (B) Ag–MUA NPs.

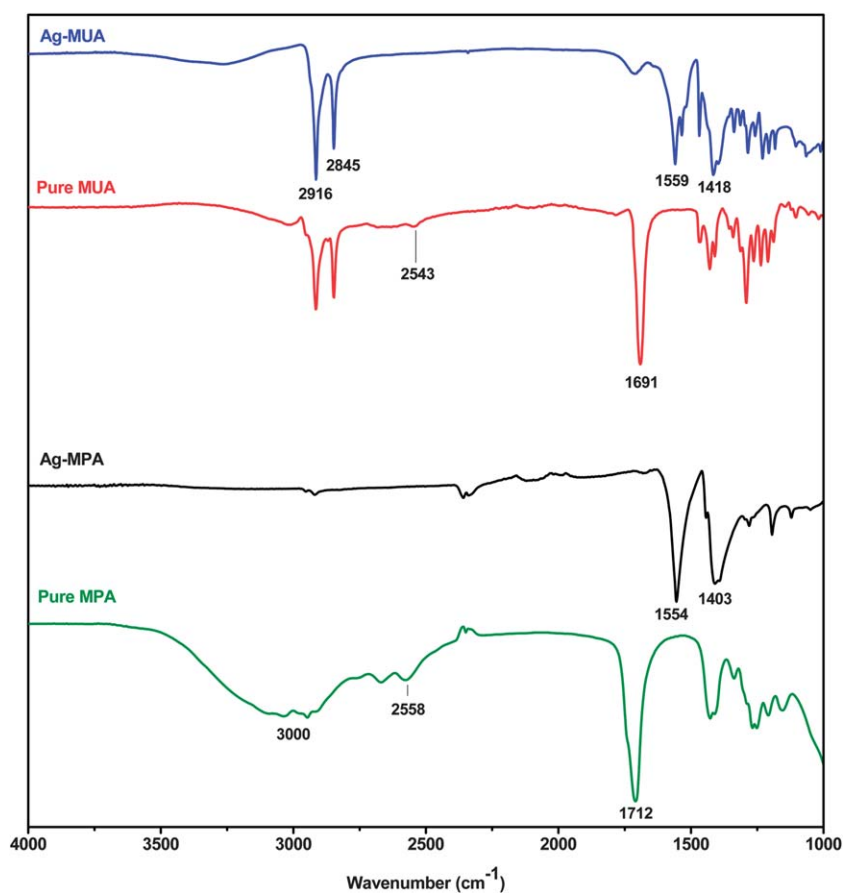


Fig. 5 FTIR spectra of pure acids MUA and MPA and the corresponding stabilized silver NPs.

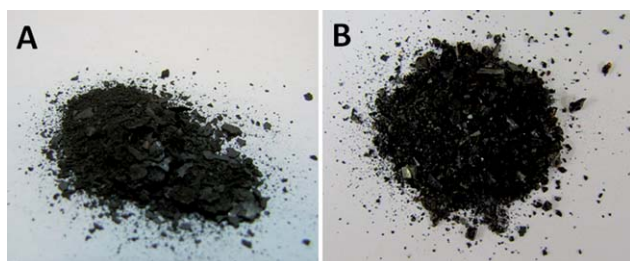


Fig. 6 Photos of dry powders of (A) Ag-MPA and (B) Ag-MUA NPs.

that is, the Ag-MUA NPs have a higher coverage of the organic layers than Ag-MPA NPs.

To obtain quantitative information, we estimated the number of functional groups per unit surface area from the weight-loss due to the decomposition of the chemisorbed acids. First, we calculated the mass of an individual NP (w_s) using the average diameter (d) of each NP (consequently volume of each NP, V), obtained from TEM images, and the density of silver (ρ).

$$V = \frac{\pi d^3}{6} \quad (2)$$

$$w_s = \rho V \quad (3)$$

Second, the total amount of organic layer in the system (W_o) was calculated using:

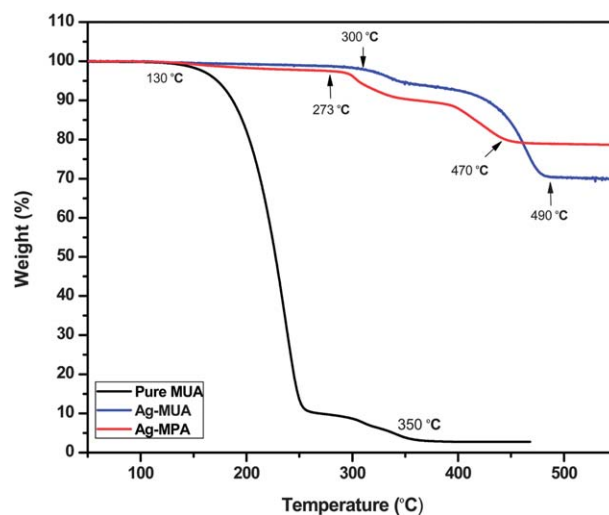


Fig. 7 Thermogravimetric curves of pure MUA, MPA and MUA stabilized-silver NPs (or Ag-MPA and Ag-MUA).

$$W_o = W\phi \quad (4)$$

where W is the total mass of each sample subjected to the TGA, and ϕ is the weight fraction of chemisorbed acid on the surface of NPs, which were 24 wt% for Ag-MUA and 11 wt% for Ag-MPA. The total amount of pure silver (W_s) in the system is obtained as:

$$W_s = W - W_o \quad (5)$$

Third, the total number of NPs (N) for each sample subjected to TGA test is determined.

$$N = \frac{W_s}{w_s} \quad (6)$$

Fourth, the average number of functional groups or chains on an individual NP was determined.

$$n = \frac{W_o}{M_w N} N_a \quad (7)$$

where M_w is the molecular weight of MPA or MUA, and N_a is the Avogadro number. $n = 42$ for Ag-MPA while $n = 409$ for Ag-MUA. Finally, the number of functional groups per unit surface area of the NP or the number density was determined.

$$n_o = \frac{n}{\pi d^2} \quad (8)$$

$n_o \approx 2.6 \text{ nm}^{-2}$ for Ag-MPA, and $n_o \approx 6.4 \text{ nm}^{-2}$ for Ag-MUA. Thus, the long-chain functional groups grafted on NP are much denser than the short-chain functional groups.

Electrical properties of functionalized NPs and the polymer composite

The electrical properties of the Ag-MUA and Ag-MPA were investigated by measuring the bulk resistivity of a sheet of NPs of 0.1 mm thick prepared by drying the dispersion of NPs in water on a microscope glass slide. Interestingly, Ag-MUA NPs did not show any conductivity whereas the bulk resistivity of the sheet of Ag-MPA NPs was around $1.02 \times 10^{-3} \Omega \text{ cm}$. According to the information extracted from TGA results, the number density of the organic chains covering the surface of Ag-MUA is almost 3 times larger than that of Ag-MPA NPs. It seems that the denser and longer chains on Ag-MUA may have assembled on the surface into a crystalline structure as implied from the FTIR analysis, effectively insulating the silver particles; on the other hand, the shorter chain and lower density of the covering layer allow Ag-MPA NPs to still be conductive. In order to understand how chemically stabilized NPs influence the overall electrical conductivity of their polymer composites, they were added into a silver flakes filled epoxy matrix at varied weight fractions to make a "hybrid" conductive adhesive. Due to the insulating nature of Ag-MUA, only Ag-MPA NPs were added to the system. The bulk resistivities of the conventional conductive adhesive containing only silver flakes at weight fractions (60–70%) near the percolation threshold value were measured as a control for the hybrid adhesive. Fig. 8 shows bulk resistivity as a function of the total weight fractions of silver fillers for both types of nanocomposites (Table 2). As can be seen in Fig. 8, in the system consisting of only silver flakes, addition of more fillers decreased bulk resistivity; however, in the nano/micro hybrid filler system, in which the total amount of flakes was kept constant, the addition of a small amount of silver NPs less than 20 wt% of the silver flakes (*i.e.* the weight fraction of NPs to silver flakes $K = 0.2$) reduced the resistivity of the nanocomposites by two orders of magnitude, while resistivity started to increase by adding more NPs (*i.e.*, $K = 0.4$ and 0.6), indicating that the NPs

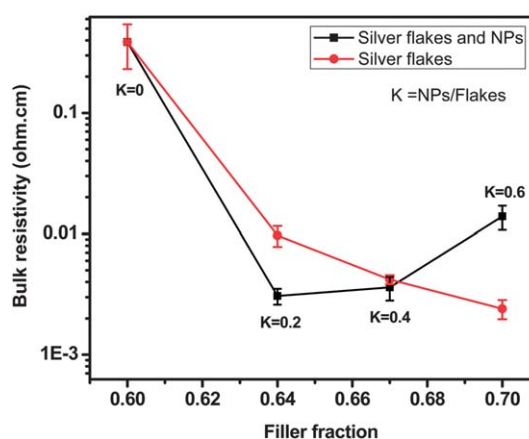


Fig. 8 Bulk resistivity of conductive adhesives as a function of filler fraction for both the micro/nano hybrid configuration (■) and conventional adhesives filled only with micron silver flakes (●). K is the weight fraction of NPs relative to the silver flakes.

played a complex role in the system. For a sample with $K = 0.4$, resistivity increased slightly as compared to a sample with $K = 0.2$, but still lower than the bulk resistivity of the conventional ECA (epoxy and silver flakes) with the same filler concentration. The addition of more NPs (*i.e.*, $K = 0.6$) further increased resistivity to a value higher by one order of magnitude than that of the conventional ECA with the same filler concentration. In other words, the hybrid adhesive outperformed the conventional adhesive at the total weight fractions between 60 and 67% ($K = 0.2$, and 0.4) while adding more NPs did not improve conductivity but resulted in higher bulk resistivity than the conventional adhesive.

To obtain some insights into the behaviour of Ag-MPA NPs in the conductive composite, SEM images of the NPs and their nanocomposites were examined and discussed in terms of the effect of NPs on the overall conductivity of the nanocomposites. The performance of a conductive adhesive depends significantly on the quality of conductive fillers and filler network. The overall electrical conductivity of the filler networks in the adhesive matrix is determined by the intrinsic resistance of the fillers and the contact resistance of the neighbouring fillers. As for the filler–filler contact resistance, it is composed of two distinct resistances: constriction resistance and tunnelling resistance.⁵¹ The former is related to the flow of electrons through contact points; the smaller number of contact points, the lower constriction resistance. It was observed that the addition of NPs into the conventional conductive adhesive has a negative effect on the overall electrical conductivity because of the increased number of contact points unless the silver NPs were sintered at elevated temperature. Therefore, we suspected that the added Ag-MPA NPs might be partially fused during curing because of their small sizes even though no particular sintering process was applied. The SEM images, shown in Fig. 9A and B, confirmed that sintering occurred between NPs and silver flakes. Although the sintering of chemically stabilized silver NPs larger than 50 nm is not expected at this annealing condition (100 °C for 1 h), the Ag-MPA NPs' small size (<5 nm) and short chain coverage may have allowed them to sinter at this relatively low temperature.

Table 2 Comparison of the bulk resistivity of different types of silver fillers

Material	Number of chains on the surface of each NPs	Number of chains per unit of surface area	Bulk resistivity (Ω cm)
Ag flakes	—	—	1.59×10^{-6}
Ag-MUA	409	6.4	—
Ag-MPA	42	2.6	1.02×10^{-3}

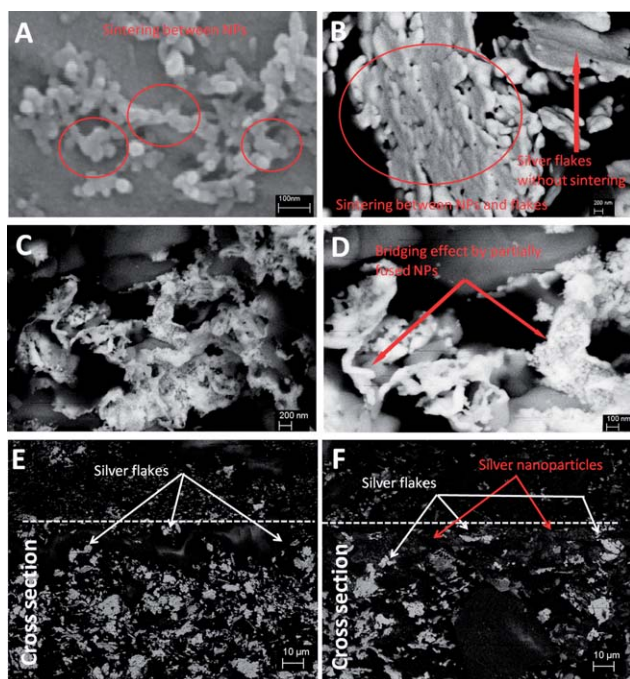


Fig. 9 SEM images of (A) sintered Ag-MPA NPs at 100 °C for 1 h; (B) sintering of NPs in the nanocomposite structure after curing at 150 °C for 2 h; (C) bridging effect of NPs between the silver flakes at lower magnification and (D) higher magnification; and 45° views of the top and cross-section of a fractured composite: (E) separated silver flakes at the surface of composites without NPs; and (F) filling of silver NPs into the gaps between the silver flakes creating new electrical paths.

Adding a small amount of Ag-MPA may help reduce the tunnelling resistance, which has been regarded as the dominant factor affecting the overall resistance of ECAs.^{51,52} Tunnelling resistance is associated with resistivity induced by the insulating materials including the surface layer of organics coated on fillers or polymeric matrix.⁵¹ One reason for the negative effect of NPs (>50 nm) on the overall electrical conductivity is that they hinder the effective contacts between silver flakes and increase the tunnelling resistance.⁵³ However, for 2 nm Ag-MPA NPs, we showed in Fig. 9C and D that they filled the gaps between silver flakes and partially fused, which bridged the originally separated flakes. This bridging effect can significantly reduce the tunnelling resistance. Furthermore, the partially fused NPs may also decrease the tunnelling resistance by creating new electrical paths throughout the epoxy. Fig. 9E and F show SEM images of the composites before and after the addition of silver NPs (weight fraction of NPs to silver flakes, $K = 0.2$). The area above the dash line is the top surface; the area beneath the dash line is the cross-section of a fractured composite. As pointed by the arrows,

clusters of NPs filled the interstices of silver flakes and made the fillers distribute more uniformly in the epoxy. Indeed, we observed in the four-probe measurements that the addition of NPs made the conventional micro-composite adhesive more electrically homogeneous. In other words, the NPs filled the gap between silver flakes and provided more electrically conductive paths. Finally, adding a larger amount of NPs ($K = 0.4$ and 0.6) may backfire because they form more and larger clusters, which may increase the gap between the silver flakes and consequently increase the tunnelling resistance. It is reasonable to conclude from these research findings that the chemically stabilized NPs can improve the electrical conductivity of the conventional ECAs at a relatively low curing temperature of 150 °C without the extra step of sintering at elevated temperature. This improvement in the electrical conductivity of the ECAs at lower filler contents using the nano/micro hybrid filler system is attributed to the partial fusion of the NPs and the action of the NPs covered with the well designed surface layer to fill the gaps between separated silver flakes due to the small size. Further studies are needed to elucidate the complex behavior of NPs in the nano/micro hybrid conductive composites.

Conclusions

In summary, we synthesized novel thiocarboxylate-functionalized silver NPs (less than 5 nm) by direct reduction of silver nitrate in the presence of two different thiocarboxylic acids. The well-controlled synthesis conditions allowed for detailed investigation of the effect of the chain length of functional groups on the thermal and electrical properties of silver NPs and their polymer composites. We found that the chain length had a significant effect on the size and conductivity of the NPs; the NPs grafted with 3-carbon thiocarboxylic acid had an average size of 2.09 nm and were conductive while those with 11-carbon acid had an average size of 4.49 nm and were non-conductive. TGA analyses revealed the number density of short-chain acids, grafted on silver NP, were about three times smaller than that of long-chain acids. The FTIR analysis indicated the long-chain acids might assemble into a crystalline structure on the surface of NPs. It was proposed that the higher surface coverage and crystalline structure of long-chain acids account for the non-conductive nature of the functionalized silver NPs. The short-chain functionalized NPs were incorporated into a hybrid-designed composite adhesive, consisting of micron-sized silver particles and the NPs in epoxy matrix. The electrical conductivity measurements and SEM images of the cross-sections of cured hybrid composites showed that low NPs contents increased electrical conductivity due to NPs filling into the interstices of the microparticles and to their low sintering temperature, whereas

higher NPs contents reduced the electrical conductivity because they clustered and increased the gaps among the micro-particles. The relationship between the properties of the nanocomposites and the surface chemistry, size and amount of NPs was discussed, showing the complex role of NPs in the nanocomposites.

Acknowledgements

This work was supported by research funds from the Natural Sciences and Engineering Research Council of Canada (NSERC). We thank Mr Fred Pearson from the Canadian Center for Electron Microscopy, McMaster University for help with TEM observation.

References

- M. Cherrington, T. C. Claypole, D. Deganello, I. Mabbett, T. Watson and D. Worsley, *J. Mater. Chem.*, 2011, **21**, 7562.
- R. N. Das, F. D. Egitto and V. R. Markovich, *Circuit World*, 2008, **34**, 3.
- J. Liu, X. Li and X. Zeng, *J. Alloys Compd.*, 2010, **494**, 84.
- Y. Long, J. Wu, H. Wang, X. Zhang, N. Zhao and J. Xu, *J. Mater. Chem.*, 2011, **21**, 4875.
- Q. Song, Y. Li, J. Xing, J. Y. Hu and Y. Marcus, *Polymer*, 2007, **48**, 3317.
- R. Brenier, *J. Phys. Chem. C*, 2012, **116**, 5358.
- M. Farrag, M. Thamer, M. Tschurl, T. Burgi and U. Heiz, *J. Phys. Chem. C*, 2012, **116**, 8034.
- A. Saxena, R. M. Tripathi, F. Zafar and P. Singh, *Mater. Lett.*, 2012, **67**, 91.
- R. Bryaskova, D. Pencheva, G. M. Kale, U. Lad and T. Kantardjiev, *J. Colloid Interface Sci.*, 2010, **349**, 77.
- M. Layani and S. Magdassi, *J. Mater. Chem.*, 2011, **21**, 15378.
- M. J. Yim, Y. Li, K. Moon, K. W. Paik and C. P. Wong, *J. Adhes. Sci. Technol.*, 2008, **22**, 1593.
- F. Liu and J. M. Nunzi, *Appl. Phys. Lett.*, 2011, **99**, 123302.
- J. C. Ramos, A. Ledezma, E. Arias, I. Moggio, C. A. Martínez and F. Castillon, *Vacuum*, 2010, **84**, 1244.
- J. Jiang, K. Moon, Y. Li and C. P. Wong, *Chem. Mater.*, 2006, **18**, 2969.
- R. Zhang, K. S. Moon, W. Lin, J. C. Agar and C. P. Wong, *Compos. Sci. Technol.*, 2011, **71**, 528.
- R. Zhang, K. Y. Moon, W. Lin and C. P. Wong, *J. Mater. Chem.*, 2010, **20**, 2018.
- Y. Li, K. S. Moon and C. P. Wong, *Mater. Sci.*, 2005, **308**, 1419.
- Y. Li and C. P. Wong, *Mater. Sci. Eng., R*, 2006, **51**, 1.
- S. Böhm, E. S. Tammen, G. Hemken and M. Wagner, in *Microjoining and Nanojoining*, ed. Y. Zhou, CRC Press, NW, USA, 2008, ch. 17, p. 500.
- W. J. Jeong, H. Nishikaw, D. Itou and T. Takemoto, *Mater. Trans.*, 2005, **46**, 2276.
- R. Zhang, J. C. Agar and C. P. Wong, *Electronics Packaging Technology Conference, 12th Proceedings*, 2010, 696.
- L. R. Bao, B. Wei and A. Y. Xiao, *Electronic Components and Technology Conference, 57th Proceedings*, 2007, 494.
- H. Gao, L. Liu, K. Liu, Y. Luo, D. Jia and J. Lu, *J. Mater. Sci.: Mater. Electron.*, 2011, **23**, 22.
- L. Ye, Z. H. Lai, J. Liu and A. Tholen, *IEEE Trans. Electron. Packag. Manuf.*, 1999, **22**, 299.
- Y. Oh, K. Y. Chun, E. Lee, Y. J. Kim and S. Baik, *J. Mater. Chem.*, 2010, **20**, 3579.
- R. Zhang, W. Lin, K. S. Moon and C. P. Wong, *ACS Appl. Mater. Interfaces*, 2010, **2**, 2637.
- P. Peng, A. Hu, H. Huang, A. P. Gerlich, B. Zhao and Y. N. Zhou, *J. Mater. Chem.*, 2012, **22**, 12997.
- M. Maskovits and J. S. Suh, *J. Am. Chem. Soc.*, 1985, **107**, 6826.
- A. Hu, J. Y. Guo, H. Alarifi, G. Patane, Y. Zhou, G. Compagnini and C. X. Xu, *Appl. Phys. Lett.*, 2010, **97**, 153117.
- C. Shen, C. Hui, T. Yang, C. Xiao, J. Tian, L. Bao, S. Chen, H. Ding and H. Gao, *Chem. Mater.*, 2008, **20**, 6939.
- C. J. Sandroff, S. Garoff and K. P. Leung, *Chem. Phys. Lett.*, 1983, **96**, 547.
- C. D. Bain, E. B. Troughtoyt, Y. T. Tao, J. E. George, M. Whitesides and R. G. Nuzzo, *J. Am. Chem. Soc.*, 1989, **111**, 321.
- M. Brust, M. Walker, D. Bethell, D. J. Schiffrin and R. Whyman, *J. Chem. Soc., Chem. Commun.*, 1994, 801.
- Q. Zhang, J. Xie, Y. Yu and J. Y. Lee, *Nanoscale*, 2010, **2**, 1962.
- A. N. Parikh, S. D. Gillmor, J. D. Beers, K. M. Beardmore, R. W. Cutts and B. I. Swanson, *J. Phys. Chem. B*, 1999, **103**, 2850.
- M. D. Malinsky, K. L. Kelly, G. C. Schatz and R. P. Van Duyne, *J. Am. Chem. Soc.*, 2001, **123**, 1471.
- J. C. Love, L. A. Estroff, J. K. Kriebel, R. G. Nuzzo and G. M. Whitesides, *Chem. Rev.*, 2005, **105**, 1103.
- S. Chen and K. Kimura, *Langmuir*, 1999, **15**, 1075.
- S. Chen and K. Kimura, *Chem. Lett.*, 1999, 1169.
- C. Ma and J. M. Harris, *Langmuir*, 2012, **28**, 2628.
- I. Dell'Erba, C. Hoppe and R. Williams, *Langmuir*, 2010, **26**, 2042.
- T. Yonezawa, M. Sutoh and T. Kunitake, *Chem. Lett.*, 1997, 619.
- A. Moores and F. Goettmann, *New J. Chem.*, 2006, **30**, 1121.
- L. Kvittek, A. Panacek, J. Soukupova, M. Kolar, R. Vecerova, R. Prucek, M. Holecova and R. Zboril, *J. Phys. Chem. C*, 2008, **112**, 5825.
- A. Henglein and D. Meisel, *J. Phys. Chem. B*, 1998, **102**, 8364.
- S. He, J. Yao, P. Jiang, D. Shi, H. Zhang, S. Xie, S. Pang and H. Gao, *Langmuir*, 2001, **17**, 1571.
- Y. Badr, M. G. Abd El Wahed and M. A. Mahmoud, *Appl. Surf. Sci.*, 2006, **253**, 2502.
- A. Manna and B. D. Kulkarni, *Chem. Mater.*, 1997, **9**, 3032.
- L. A. Porter Jr, D. Ji, S. L. Westcott, M. Graupe, R. S. Czernuszewicz, N. J. Halas and T. R. Lee, *Langmuir*, 1998, **14**, 7378.
- D. E. Cliffl, F. P. Zamborini, S. M. Gross and R. W. Murray, *Langmuir*, 2000, **16**, 9699.
- G. R. Ruschau, S. Yoshikawa and R. E. Newnham, *J. Appl. Phys.*, 1992, **72**, 953.
- J. C. Agar, K. J. Lin, R. Zhang, J. Durden, K. Lawrence, K. S. Moon, C. P. Wong, *Electronic Components and Technology Conference, 60th Proceedings*, 2010, 1713.
- H. H. Lee, K. S. Choua and Z. W. Shih, *Int. J. Adhes. Adhes.*, 2005, **25**, 437.